JOC Article
pubs.acs.org/joc

Proof for the Concerted Inversion Mechanism in the *trans* → *cis* Isomerization of Azobenzene Using Hydrogen Bonding To Induce Isomer Locking

H. M. Dhammika Bandara,[†] Tracey R. Friss,[†] Miriam M. Enriquez,[†] William Isley,[†] Christopher Incarvito,[‡] Harry A. Frank,[†] Jose Gascon,[†] and Shawn C. Burdette*,[†]

[†]*Department of Chemistry, University of Connecticut, 55 North Eagleville Road U-3060, Storrs, Connecticut 06269, and* [‡]*Department of Chemistry, Yale University, 225 Prospect Street, P.O. Box 208107, New Haven, Connecticut 06520-8107*

shawn.burdette@uconn.edu

Received May 4, 2010

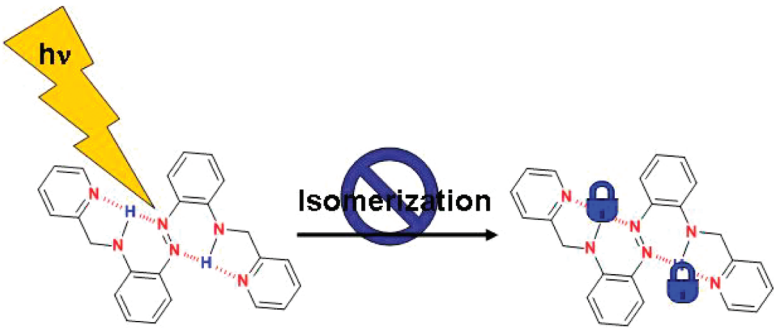

Azobenzene undergoes reversible *cis*↔*trans* photoisomerization upon irradiation. Substituents often change the isomerization behavior of azobenzene, but not always in a predictive manner. The synthesis and properties of three azobenzene derivatives, AzoAMP-1, -2, and -3, are reported. AzoAMP-1 (2,2′-bis[*N*-(2-pyridyl)methyl]diaminoazobenzene), which possesses two aminomethylpyridine groups *ortho* to the azo group, exhibits minimal *trans*→*cis* photoisomerization and extremely rapid *cis*→*trans* thermal recovery. AzoAMP-1 adopts a planar conformation in the solid state and is much more emissive (Φ_{fl} = 0.003) than azobenzene when frozen in a matrix of 1:1 diethylether/ethanol at 77 K. Two strong intramolecular hydrogen bonds between anilino protons and pyridyl and azo nitrogen atoms are responsible for these unusual properties. Computational data predict AzoAMP-1 should not isomerize following S_2←S_0 excitation because of the presence of an energy barrier in the S_1 state. When potential energy curves are recalculated with methyl groups in place of anilino protons, the barrier to isomerization disappears. The dimethylated analogue AzoAMP-2 was independently synthesized, and the photoisomerization predicted by calculations was confirmed experimentally. AzoAMP-2, when irradiated at 460 nm, photoisomerizes with a quantum yield of 0.19 and has a much slower rate of thermal isomerization back to the *trans* form compared to that of AzoAMP-1. Its emission intensity at 77 K is comparable to that of azobenzene. Confirmation that the AzoAMP-1 and -2 retain excited state photochemistry analogous to azobenzene was provided by ultrafast transient absorption spectroscopy of both compounds in the visible spectral region. The isomerization of azobenzene occurs via a concerted inversion mechanism where both aryl rings must adopt a collinear arrangement prior to inversion. The hydrogen bonding in AzoAMP-1 prevents both aryl rings from adopting this conformation. To further probe the mechanism of isomerization, AzoAMP-3, which has only one anilinomethylpyridine substituent for hydrogen bonding, was prepared and characterized. AzoAMP-3 does not isomerize and exhibits emission (Φ_{fl} = 0.0008) at 77 K. The hydrogen bonding motif in AzoAMP-1 and AzoAMP-3 provides the first example where inhibiting the concerted inversion pathway in an azobenzene prevents isomerization. These molecules provide important supporting evidence for the spectroscopic and computational studies aimed at elucidating the isomerization mechanism in azobenzene.

DOI: 10.1021/jo100866m Published on Web 06/14/2010

Introduction

Azobenzene undergoes a reversible *trans*→*cis* conformational change upon photoexcitation,[1] which has been utilized as a light-triggered switch in a variety of polymers,[2] surface-modified materials,[3] protein probes,[4] molecular machines,[5] and metal ion chelators.[6−9] The change in geometry upon isomerization orients the molecules to perform a task,[10−12] modulates interactions that change the structure of the bulk material,[13−15] changes the spectroscopic properties,[16−19] or moves a substituent that blocks or unblocks activity.[4,20−22] Despite the prevalence of azobenzene derivatives in a broad spectrum of chemical applications, predicting the photochemical properties of azobenzene derivatives remains difficult, and the mechanism of isomerization continues to be a topic of interest.

The ground-state (S_0) absorption spectrum of *trans*-azobenzene has two well-defined bands in the UV−vis region. The symmetry-forbidden $S_1(n\pi^*)\leftarrow S_0$ transition appears as a weak band at ∼450 nm, while the symmetry-allowed $S_2(\pi\pi^*)\leftarrow S_0$ transition absorbs at ∼320 nm (Figure 1A). The *cis* isomer is thermodynamically unstable, and hence *cis* to *trans* thermal isomerization occurs in the dark; however, thermal isomerization proceeds more slowly than photoisomerization.[23] Excitation to both S_1 and S_2 states leads to the *trans*→*cis* transformation, but the S_1 state relaxes to the ground state with a higher quantum yield of isomerization.[1,24] Original investigators of azobenzene photochemistry suggested that isomerization from the S_1 state occurred by in-plane inversion centered at one of the azo-N atoms, whereas isomerization from the S_2 state resulted from an out-of-plane rotation after scission of the N=N π-bond (Figure 1B).[25] The excitation wavelength dependence of the isomerization quantum yield was attributed to the different isomerization mechanisms.

The dual isomerization mechanism was discarded when femtosecond time-resolved spectroscopic studies revealed that $S_1\leftarrow S_2$ occurs with a quantum yield of ∼1, an efficiency that precludes isomerization from the S_2 state.[26] Azobenzenes with rotation about the N−N bond restricted by steric constraints have quantum yields of isomerization independent of the excitation wavelength,[27,28] which suggests photoisomerization from the S_1 state dominates regardless of the initial excited state.

Recent computational studies suggest that excitation of azobenzene to the S_1 state is followed by isomerization through rotation.[29−31] Excitation to the S_2 state is followed by rapid relaxation to the S_1 state. The isomerization and return to the S_0 state occurs through a concerted-inversion mechanism that involves simultaneous distortions of both N−N−C bonds (Figure 1B).[29] The lifetime of the S_1 state generated by the relaxation of the S_2 state is 500 fs,[26] but the S_1 state prepared by direct $S_1\leftarrow S_0$ excitation has a longer lifetime of 2.6 ps.[32] The $S_1\leftarrow S_2$ crossover creates a vibrationally excited S_1 state that relaxes rotationally to the *trans* isomer resulting in a lower quantum yield of isomerization. The quantum yield of isomerization also decreases with increasing vibrational energy in the $S_1\leftarrow S_0$ inversion pathway. Irradiation of the *trans* isomer with 436 nm radiation results in a quantum yield of isomerization of 0.27, which decreases to 0.21 with 405 nm radiation.[24] Both theoretical and experimental evidence suggest that isomerization always occurs from the S_1 state; however, additional isomerization channels are opened when the S_1 state is accessed by the relaxation of the S_2 state. Theoretical studies have suggested that such additional isomerization channel must involve a concerted inversion pathway, where both the C−N=N and N=N−C angles change simultaneously.[29,33]

Azobenzene exhibits very weak fluorescence emission due to deactivation of the excited state by isomerization. Azobenzene does not obey Kasha's rule, but at room temperature the $S_0\leftarrow S_1$ quantum yield of fluorescence is 2.53×10^{-5}.[26] An increase in emission intensity can be observed from the $S_0\leftarrow S_2$ state in a frozen matrix when relaxation to the S_1 state is impaired.[34] Engineering bonding interactions can provide conformationally locked azobenzene derivatives that show strong fluorescence at room temperature.[35,36]

(1) Bortolus, P.; Monti, S. *J. Phys. Chem.* **1979**, *83*, 648–652.
(2) Puntoriero, F.; Ceroni, P.; Balzani, V.; Bergamini, G.; Vogtle, F. *J. Am. Chem. Soc.* **2007**, *129*, 10714–10719.
(3) Ferri, V.; Elbing, M.; Pace, G.; Dickey, M. D.; Zharnikov, M.; Samori, P.; Mayor, M.; Rampi, M. A. *Angew. Chem., Int. Ed.* **2008**, *47*, 3407–3409.
(4) Banghart, M. R.; Fortin, A. M. D. L.; Yao, J. Z.; Kramer, R. H.; Trauner, D. *Angew. Chem., Int. Ed.* **2009**, *48*, 9097–9101.
(5) Muraoka, T.; Kinbara, K.; Aida, T. *Nature* **2006**, *440*, 512–515.
(6) Evangelio, E.; Saiz-Poseu, J.; Maspoch, D.; Wurst, K.; Busque, F.; Ruiz-Molina, D. *Eur. J. Inorg. Chem.* **2008**, 2278–2285.
(7) Shinkai, S.; Nakaji, T.; Nishida, Y.; Ogawa, T.; Manabe, O. *J. Am. Chem. Soc.* **1980**, *102*, 5860–5865.
(8) Luboch, E.; Wagner-Wysiecka, E.; Poleska-Muchlado, Z.; Kravtsov, V. C. *Tetrahedron* **2005**, *61*, 10738–10747.
(9) Luboch, E.; Wagner-Wysiecka, E.; Rzymowski, T. *Tetrahedron* **2009**, *65*, 10671–10679.
(10) Cacciapaglia, R.; Di Stefano, S.; Mandolini, L. *J. Am. Chem. Soc.* **2003**, *125*, 2224–2227.
(11) Stoll, R. S.; Hecht, S. *Org. Lett.* **2009**, *11*, 4790–4793.
(12) Stoll, R. S.; Peters, M. V.; Kuhn, A.; Heiles, S.; Goddard, R.; Buhl, M.; Thiele, C. M.; Hecht, S. *J. Am. Chem. Soc.* **2009**, *131*, 357–367.
(13) Yamada, M.; Kondo, M.; Miyasato, R.; Naka, Y.; Mamiya, J.; Kinoshita, M.; Shishido, A.; Yu, Y. L.; Barrett, C. J.; Ikeda, T. *J. Mater. Chem.* **2009**, *19*, 60–62.
(14) Zhang, Q.; Bazuin, C. G. *Macromolecules* **2009**, *42*, 4775–4786.
(15) Kumar, S. K.; Pennakalathil, J.; Kim, T. H.; Kim, K.; Park, J. K.; Hong, J. D. *Langmuir* **2009**, *25*, 1767–1771.
(16) Khan, A.; Hecht, S. *Chem.—Eur. J.* **2006**, *12*, 4764–4774.
(17) Khan, A.; Hecht, S. *J. Polym. Sci. A* **2006**, *44*, 1619–1627.
(18) Khan, A.; Kaiser, C.; Hecht, S. *Angew. Chem., Int. Ed.* **2006**, *45*, 1878–1881.
(19) Mathews, M.; Tamaoki, N. *J. Am. Chem. Soc.* **2008**, *130*, 11409–11416.
(20) Banghart, M.; Borges, K.; Isacoff, E.; Trauner, D.; Kramer, R. H. *Nat. Neurosci.* **2004**, *7*, 1381–1386.
(21) Gorostiza, P.; Volgraf, M.; Numano, R.; Szobota, S.; Trauner, D.; Isacoff, E. Y. *Proc. Natl. Acad. Sci. U.S.A.* **2007**, *104*, 10865–10870.
(22) Volgraf, M.; Gorostiza, P.; Numano, R.; Kramer, R. H.; Isacoff, E. Y.; Trauner, D. *Nat. Chem. Biol.* **2006**, *2*, 47–52.
(23) Blevins, A. A.; Blanchard, G. J. *J. Phys. Chem. B* **2004**, *108*, 4962–4968.
(24) Zimmerman, G.; Chow, L.-Y.; Paik, U.-J. *J. Am. Chem. Soc.* **1958**, *80*, 3528–3531.
(25) Monti, S.; Orlandi, G.; Palmieri, P. *Chem. Phys.* **1982**, *71*, 87–99.
(26) Fujino, T.; Arzhantsev, S. Y.; Tahara, T. *J. Phys. Chem. A* **2001**, *105*, 8123–8129.
(27) Rau, H.; Lueddecke, E. *J. Am. Chem. Soc.* **1982**, *104*, 1616–1620.
(28) Lednev, I. K.; Ye, T.-Q.; Abbott, L. C.; Hester, R. E.; Moore, J. N. *J. Phys. Chem. A* **1998**, *102*, 9161–9166.
(29) Crecca, C. R.; Roitberg, A. E. *J. Phys. Chem. A* **2006**, *110*, 8188–8203.
(30) Ishikawa, T.; Noro, T.; Shoda, T. *J. Chem. Phys.* **2001**, *115*, 7503–7512.
(31) Tiago, M. L.; Ismail-Beigi, S.; Louie, S. G. *J. Chem. Phys.* **2005**, *122*, 094311.
(32) Lednev, I. K.; Ye, T. Q.; Matousek, P.; Towrie, M.; Foggi, P.; Neuwahl, F. V. R.; Umapathy, S.; Hester, R. E.; Moore, J. N. *Chem. Phys. Lett.* **1998**, *290*, 68–74.
(33) Diau, E. W. G. *J. Phys. Chem. A* **2004**, *108*, 950–956.
(34) Nepras, M.; Lunak, S., Jr.; Hrdina, R.; Fabian, J. *Chem. Phys. Lett.* **1989**, *159*, 366–370.
(35) Yoshino, J.; Furuta, A.; Kambe, T.; Itoi, H.; Kano, N.; Kawashima, T.; Ito, Y.; Asashima, M. *Chem.—Eur. J.* **2010**, *16*, 5026–5035.

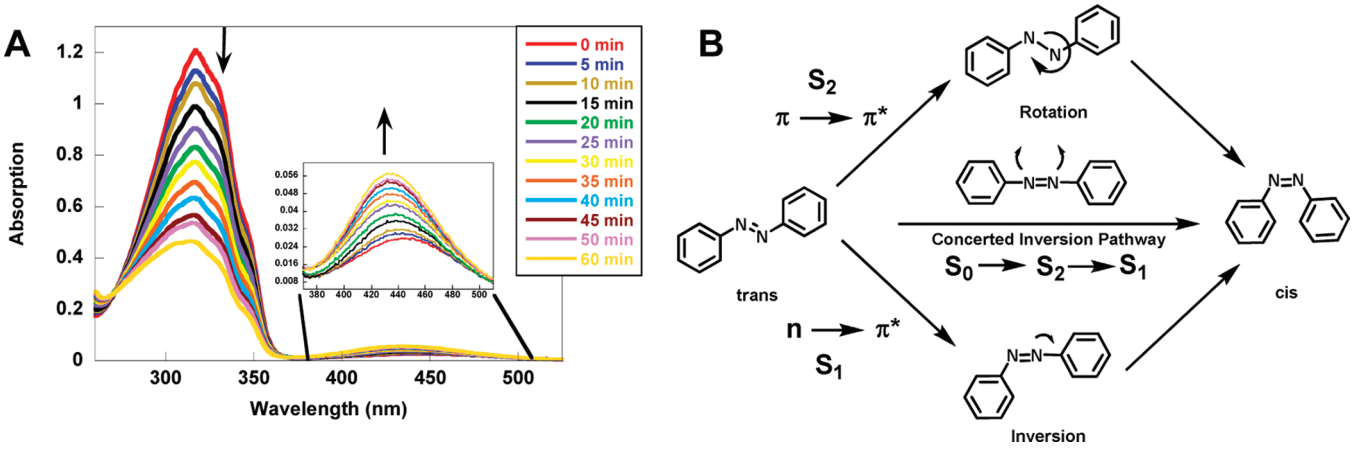

FIGURE 1. (A) Changes in the absorption spectrum of azobenzene upon irradiation with 320 nm light. The $S_1(n\pi^*)\leftarrow S_0$ transition appears as a weak band at ~440 nm (inset) and the $S_2(\pi\pi^*)\leftarrow S_0$ transition absorbs at ~320 nm. (B) Historic erroneously presumed azobenzene isomerization pathways upon S_1 (bottom) and S_2 (top) excitation and the currently accepted concerted inversion isomerization mechanism (center) following S_2 excitation that is supported by time-resolved spectroscopy and theoretical studies.

Several studies have attempted to use steric congestion around the azo group to inhibit isomerization and enhance fluorescence emission.[37,38] Hydrogen bonding has been reported to enhance the emission of 2-hydroxyazobenzene and related derivatives, but not the aniline analogues.[39] Metal binding induces emission enhancement of 2,2′dihydroxyazobenzene;[40,41] however, these compounds tautomerize readily unlike other azobenzene derivatives and therefore exhibit different photochemistry.[42]

On the basis of the light-driven changes in metal ion binding observed with crown ether-azobenzene dyads, we envisioned a ligand with light-tunable affinity for metal ions based on 2,2′-diaminoazobenzene. Installing a pyridylmethyl group on each aniline nitrogen atom would provide a binding pocket that could accommodate different metal complexes in each isomeric form. Preliminary modeling studies suggested that in the *trans* conformation, the azobenzene would provide a prearranged structure with a higher affinity for Zn^{2+}; however, canting of the aryl rings in the *cis* conformer would prevent simultaneous binding of the guest by both halves of the ligand. With the objective of developing new applications for photoisomerizable metal ion chelators, we initiated a synthetic and spectroscopic study of these ligands. In the course of our investigation, we discovered some unusual and unexpected photochemistry of *ortho* disubstituted derivatives that has provided insight into underlying aspects of azobenzene isomerization as well as the possibility to uncover new applications for a well-known molecule.

Results and Discussion

Design and Photochemistry of AzoAMP-1. The use of 2,2′-disubstituted azobenzene scaffold was inspired in part by a Mg^{2+} chelator resembling an elongated EDTA motif.[43] The Mg^{2+} ligand incorporated iminodiacetate ligands on two of the carbon atoms adjacent to the azo group. While the apo chelator exhibited the expected reversible *trans*→*cis* interconversion, no photoisomerization was observed in the presence of Mg^{2+}; in addition the parent 2,2′-diaminoazobenzene (**5**) isomerized efficiently. Since the presumed Mg^{2+} complex was coordinatively saturated, we hypothesized that eliminating one ligand from each anilino nitrogen atom would provide a less rigid metal complex that could isomerize.

The 2,2′-diaminoazobenzene ligand framework was prepared by the oxidation of *o*-phenylenediamine.[44] Initially AzoAMP-1 (2,2′-bis[*N*,*N*′-(2-pyridyl)methyl]diaminoazobenzene) was synthesized by a nucleophilic substitution reaction between **5** and 2-picholylchloride, but the desired product only was obtained in low yields. The name AzoAMP-1 is derived from the azobenzene (azo) and 2-aminomethylpyridine (AMP) components of the molecule. Alternatively, reductive amination of 2-pyridinecarboxaldehyde and **5** provided AzoAMP-1 as a red crystalline solid in 30.1% yield (Scheme 1A). Only the more thermodynamically stable *trans* isomer was observed by ^{1}H NMR spectroscopy.

The λ_{max} of the $S_2\leftarrow S_0$ transition of AzoAMP-1 appears at 490 nm compared to 320 in unsubstituted azobenzene. The large bathochromic shift of the transition compared to the parent chromophore indicates a significant delocalization of the anilino lone pair into the π-system, which is typical of diaminoazobenzenes.[23] To interrogate the photochemistry, a solution of AzoAMP-1 was irradiated with a 150 W Xe lamp, and the absorbance was recorded at 10 min intervals for 4 h. Although no evidence of significant AzoAMP-1 isomerization was observed under these conditions, the isomerization of 2,2-diaminoazobenzene was reproduced in analogous experiments.[43] To further interrogate AzoAMP-1 isomerization, several organic solvents with a broad range of polarities were screened, as well as aqueous solutions with different pH ($1 < pH < 14$). In addition to the media, the excitation wavelength was varied between 250 and 600 nm, but only minimal changes in absorbance (< 10% reduction)

(36) Yoshino, J.; Kano, N.; Kawashima, T. *Chem. Commun.* **2007**, 559–561.
(37) Bunce, N. J.; Ferguson, G.; Forber, C. L.; Stachnyk, G. J. *J. Org. Chem.* **1987**, *52*, 394–398.
(38) Han, M.; Ishikawa, D.; Muto, E.; Hara, M. *J. Lumin.* **2009**, *129*, 1163–1168.
(39) Nurmukhametov, R. N.; Shigorin, D. N.; Kozlov, Y. I.; Puchkov, V. A. *Opt. Spectrosc.* **1961**, *11*, 327–330.
(40) Diehl, H.; Olsen, R.; Spielholtz, G. I.; Jensen, R. *Anal. Chem.* **1963**, *35*, 1144–1154.
(41) Freeman, D. C.; White, C. E. *J. Am. Chem. Soc.* **1956**, *78*, 2678–2682.
(42) Dedkov, Y. M.; Kotov, A. V. *Russ. Chem. Bull.* **1973**, *22*, 1334–1336.
(43) Momotake, A.; Arai, T. *Tetrahedron Lett.* **2003**, *44*, 7277–7280.
(44) Crank, G.; Makin, M. I. H. *Tetrahedron Lett.* **1979**, *20*, 2169–2170.

SCHEME 1. Synthesis of AzoAMP-1 (A), AzoAMP-2 (B), and AzoAMP-3 (C)

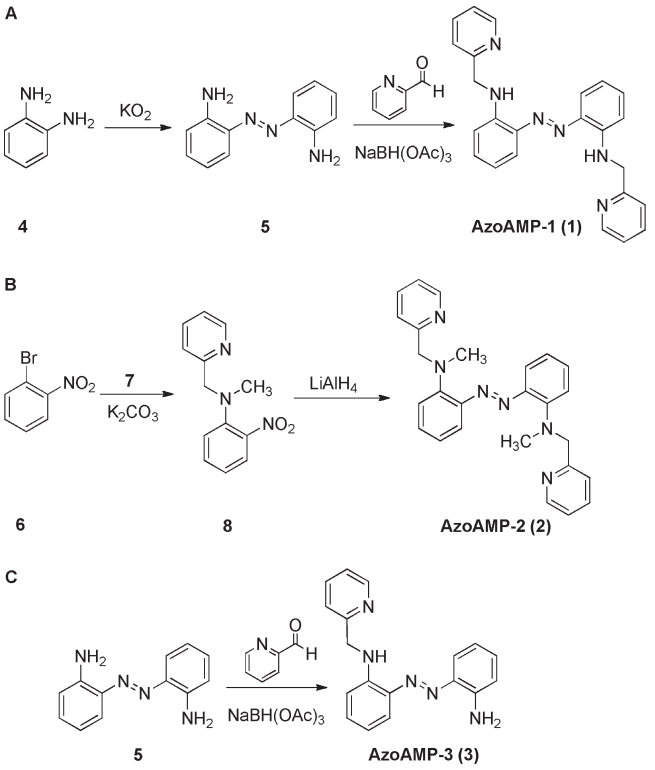

were observed even after prolonged irradiation. In addition to minimal formation of the *cis* isomer, the thermal *cis*→*trans* isomerization appears to occur within seconds, unlike 2,2′-diaminoazobenzene that takes 30 min to recover completely.

To interrogate the electronic structure of AzoAMP-1 further, spectroscopic studies were conducted on AzoAMP-1 at 77 K in a transparent glass of 1:1 EtOH/Et_2O. At room temperature azobenzene exists in a large number of conformations due to rotation around the two N−C bonds, which results in broad absorption bands. Unlike the parent compound, the disubstituted azobenzene, bis-4,4′-diethylaminoazobenzene (BDAAB), exhibits a partially resolved vibronic structure at room temperature that becomes clearer at 77 K.[34] Delocalization of the anilino lone pairs into the π-system of BDAAB causes the molecule to adopt a rigid planar conformation by preventing rotation around the N−C bonds. The vibronic structure of the AzoAMP-1 S_2←S_0 transition also becomes partially resolved when trapped in a frozen matrix, which suggests that AzoAMP-1 also exists in a rigid planar conformation.

Although AzoAMP-1 exhibits no detectable fluorescence emission at room temperature, it becomes emissive when frozen in an EtOH/Et_2O glass. The fluorescence exhibits a bimodal emission profile with an emission maximum at 566 nm and a slightly weaker peak at 602 nm (Figure 2). At room temperature, azobenzene fluorescence intensity from the S_2 and S_1 states is nearly identical.[26,45] The emission bands of azobenzene are separated significantly as is observed for the two absorption peaks. Since the two absorption bands of AzoAMP-1 are coincidental, the emission bands

(45) Fujino, T.; Arzhantsev, S. Y.; Tahara, T. *Bull. Chem. Soc. Jpn.* **2002**, *75*, 1031–1040.

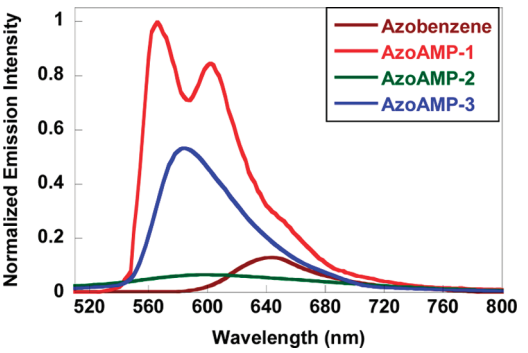

FIGURE 2. Relative emission intensity of azobenzene, AzoAMP-1, AzoAMP-2, and AzoAMP-3 in a frozen 1:1 ether/ethanol matrix. Excitation provided at the λ_{max} for each compound.

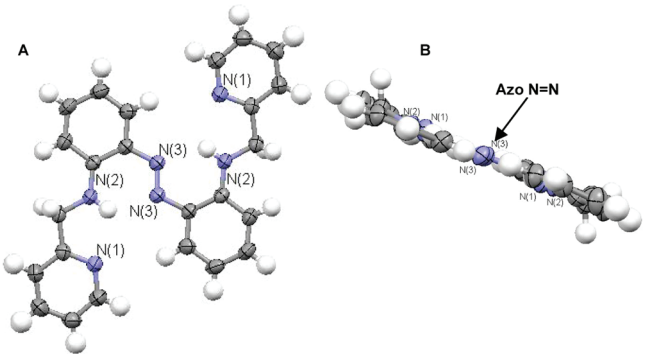

FIGURE 3. (A) ORTEP diagram of AzoAMP-1 showing 50% thermal ellipsoids and selected atom labels. (B) Side view of AzoAMP-1 showing the coplanarity of all non-hydrogen atoms.

might correspond to overlapping emission from the S_2 and S_1 states; however, additional experiments will be required to confirm this hypothesis. The emission of AzoAMP-1 is weak (Φ = 0.003) but considerably higher than the quantum yield of emission of azobenzene under the same conditions (Φ = 0.0001). The increased quantum yield of AzoAMP-1 suggests the compound adopts a more rigid conformation than azobenzene at low temperature, which prevents deactivation of the excited state by isomerization or vibration. Use of dative covalent bonding produces more emissive azobenzene derivatives;[35,36] however, weaker hydrogen bonding interactions have not been examined in this capacity.

X-ray quality crystals of AzoAMP-1 were obtained by diffusing Et_2O into CH_3OH/CH_3CN; however, AzoAMP-1 forms large single crystals under a variety of conditions. AzoAMP-1 adopts the *trans* conformation in the solid state (Figure 3). The geometry of the two anilino nitrogen atoms is trigonal planar despite formal sp^3 hybridization. Hydrogen bonding of the anilino protons to the azo and the pyridinium nitrogen atoms enforces the planar geometry; however, π-stacking in the crystal lattice reinforces this planarity. AzoAMP-1 exhibits a 5-6 chelate ring motif, where the aniline hydrogen atom coordinates to the distal azo nitrogen atom in AzoAMP-1 forming a six-membered ring instead of the proximal one that would result in a five-membered ring. The preference for adopting this structure may reflect the bite angle requirements for interaction with a hydrogen atom. The hydrogen bonds also persist in solution as indicated by the

downfield signal at ~9 ppm in the ^{1}H NMR spectrum in $CDCl_3$. The anilino protons of 2,2′-diaminoazobenzene appear at ~5.50 ppm, which indicates the significant interaction of the pyridyl hydrogen bond acceptors to strong intramolecular hydrogen bonds in AzoAMP-1. Just as electronics and steric requirements contribute to the isomerization properties of azobenzene derivatives, the hydrogen bonds enhance the thermodynamic stability of *trans*-AzoAMP-1 that provides insight into the fluorescence and isomerization behavior.

To quantify the effect of the hydrogen bonding interaction on the isomerization, we performed computational studies on AzoAMP-1 to probe the energetics of various excited states involved in the rotational, inversion, and concerted inversion isomerization pathways. Ground and excited states were obtained using density functional theory (DFT) and time-dependent DFT with the hybrid functional B3LYP and the split-valence double-ζ basis set 6-31 g**. A similar approach was recently used at the same level of theory to study the photoisomerization of azobenzene,[29] which show consistent results with respect to other wave-based *ab initio* calculations.[31,33,46−51]

For the rotation pathway, one N=N−C angle was fixed at 120° while the other angle was scanned from 0 to 180° at 10° intervals. For the inversion pathway one of the N=N−C angles was fixed at its minimum energy value in the *trans* conformation (~115°), while the dihedral C−N=N−C angle was varied from 100° to 250° at 10° intervals (Figure 4B). In the concerted inversion pathway both N=N−C angles were distorted simultaneously from 100° to 180°. The calculations reveal the absence of a probable isomerization pathway in AzoAMP-1 for the inversion and rotation pathways, which is similar to the results obtained with azobenzene.

Potential energy curves calculated previously and reproduced for this study indicate that azobenzene isomerization occurs through a concerted inversion pathway when the molecule is excited into the S_2 state. Clear conical intersections are observed between the S_1←S_2 and the S_0←S_1 states allowing the excited molecule to relax into the S_1 state with excess potential energy and return to the ground state (Figure 4A). The question arises as to whether the concerted inversion pathway is also an isomerization pathway in AzoAMP-1. The calculations on AzoAMP-1 reveal a possible conical intersection for the concerted inversion pathway although a gap exists (Figure 4B). In contrast to azobenzene however, the hydrogen bonding in AzoAMP-1 prevents the two required N=N−C distortions that bring the two aryl rings into the same plane prior to the inversion. Such a strong restraint affects rotation in both the S_0 and S_1, making the energy basin more pronounced. Thus, upon S_1←S_2 conversion around 120° the system will not have enough kinetic energy around the N=N bond to reach the potential near the S_0←S_1 intersection. Since the coplanarization prerequisite cannot be achieved, the computation predicts that AzoAMP-1 should not isomerize, which is confirmed by the spectroscopic studies.

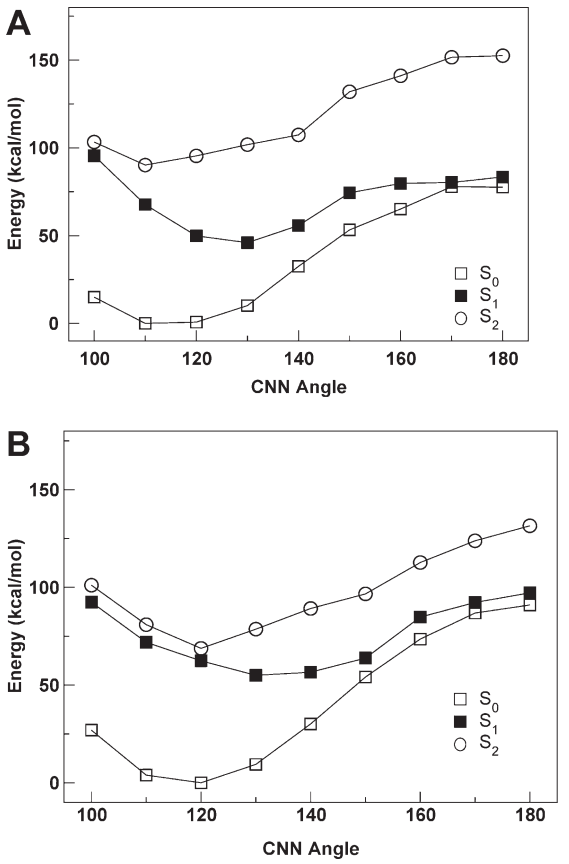

FIGURE 4. Calculated energy surfaces for the concerted inversion isomerization pathway for azobenzene (A) and AzoAMP-1 (B).

Design and Photochemistry of AzoAMP-2. Because the intramolecular hydrogen bonds in AzoAMP-1 appear to be responsible for the unusual photochemistry, we rationalized that replacing the two anilino protons with methyl groups would provide an active azobenzene. The analogous computed potential energy curves for the rotation, inversion, and concerted inversion isomerization pathways of AzoAMP-2 are similar to those of azobenzene; therefore, we predicted that AzoAMP-2 would photoisomerize by the concerted inversion when excited into the S_2 state (Figure 5).

Attempts to prepare AzoAMP-2 using AzoAMP-1 as a starting material were unsuccessful. AzoAMP-1 is highly unreactive with formaldehyde using reductive amination conditions. Strong alkylating reagents such as CH_3I failed to give the desired product by nucleophilic substitution even when used in conjunction with a strong base such as lithium diisopropylamine, so an alternative one-step preparation based on reduction of nitrobenzene derivatives was explored.[52] A nucleophilic aromatic substitution reaction between the amine **7** and 2-bromonitrobenzene (**6**) gave the nitroaniline **8** with a satisfactory yield. The nitroaniline was reduced with

(46) Biswas, N.; Umapathy, S. *J. Phys. Chem. A*. **1997**, *101*, 5555–5566.
(47) Cattaneo, P.; Persico, M. *Phys. Chem. Chem. Phys*. **1999**, *1*, 4739–4743.
(48) Cembran, A.; Bernardi, F.; Garavelli, M.; Gagliardi, L.; Orlandi, G. *J. Am. Chem. Soc*. **2004**, *126*, 3234–3243.
(49) Fliegl, H.; Kohn, A.; Hattig, C.; Ahlrichs, R. *J. Am. Chem. Soc*. **2003**, *125*, 9821–9827.
(50) Gagliardi, L.; Orlandi, G.; Bernardi, F.; Cembran, A.; Garavelli, M. *Theor. Chem. Acc*. **2004**, *111*, 363–372.
(51) Ootani, Y.; Satoh, K.; Nakayama, A.; Noro, T.; Taketsugu, T. *J. Chem. Phys*. **2009**, *131*, 194306.
(52) Tanino, T.; Yoshikawa, S.; Ujike, T.; Nagahama, D.; Moriwaki, K.; Takahashi, T.; Kotani, Y.; Nakano, H.; Shirota, Y. *J. Mater. Chem*. **2007**, *17*, 4953–4963.

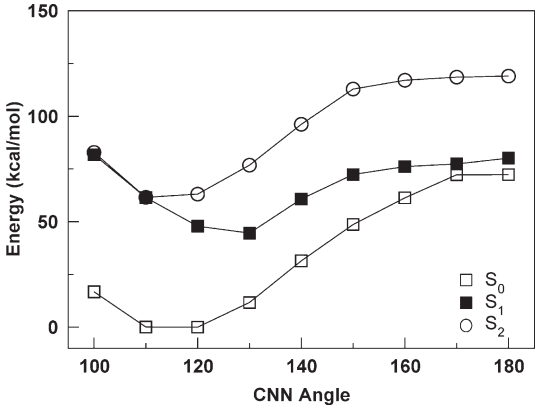

FIGURE 5. Calculated energy surfaces for the concerted inversion isomerization pathway for AzoAMP-2.

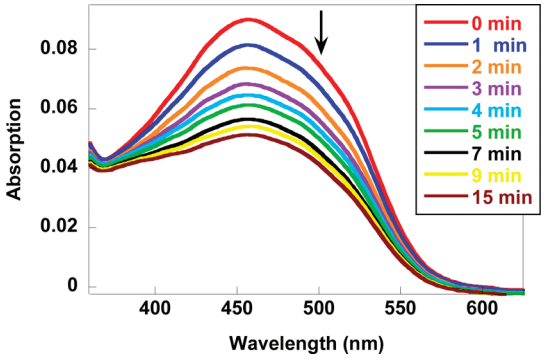

FIGURE 6. Spectroscopic changes upon irradiation of AzoAMP-2 at 451 nm. Isomerization efficiency can be measured by ^{1}H NMR.

lithium aluminum hydride to give AzoAMP-2 in moderate yields (Scheme 1B). After purification by column chromatography, only the *trans* isomer of AzoAMP-2 was observed by ^{1}H NMR spectroscopy.

The $S_2 \leftarrow S_0$ transition of AzoAMP-2 shows a large bathochromic shift and overlaps with the $S_1 \leftarrow S_0$ transition analogous to AzoAMP-1. Unlike AzoAMP-1, exposure of AzoAMP-2 at λ_{max} 460 nm results in changes in the intensity, which indicates *trans*→*cis* photoisomerization (Figure 6). TLC analysis confirms no photodegradation of AzoAMP-2, and a photostationary state was reached after 15 min of irradiation. The quantum yield of isomerization of AzoAMP-2 was determined by monitoring the changes in the ^{1}H NMR spectrum after irradiating at 460 nm for 30 min. Growth of new peaks was observed near both the NCH_3 and NCH_2Py resonances, which correspond to *cis*-AzoAMP-2. These were integrated to calculate the *trans*:*cis* isomer ratio. The quantum yield of isomerization of AzoAMP-2 was determined to be 0.19 using ferrioxalate actinometry to determine the intensity of the radiation source, which is lower than that of azobenzene under similar conditions. Infrared spectroscopy, which can measure the *trans*:*cis* isomer ratio of azobenzene, cannot be used with AzoAMP-2 because of overlapping absorption of the pyridyl groups. In the photostationary state approximately 20% of AzoAMP-2 exists in the *cis* form compared to azobenzene that exhibits 95% conversion. Steric interactions between the anilino substituents presumably contribute to the thermodynamic instability the *cis* isomer of AzoAMP-2 decreasing the conversion. Since the

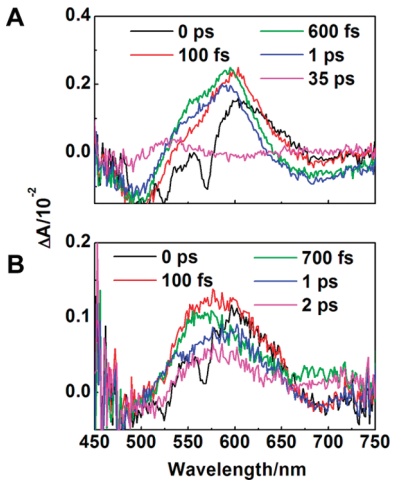

FIGURE 7. Transient absorption spectra taken at different time delays after excitation at 490 nm for AzoAMP-1 (A) and AzoAMP-2 (B).

absorption of *trans* and *cis* AzoAMP-2 overlap and the extinction coefficient of the $S_2 \leftarrow S_0$ transition of the *trans* isomer is large, it is not possible to selectively excite the *cis*→*trans* isomerization with light because the initial conversion is not complete. After reaching the photostationary state, AzoAMP-2 returns to the *trans* isomer by thermal isomerization but requires over 1 h to reach equilibrium.

No detectable fluorescence of AzoAMP-2 was observed at room temperature, and the emission at 77 K is significantly weaker than the intensity measured for AzoAMP-1 but comparable to that of azobenzene. This observation suggests that AzoAMP-2 adopts a less rigid conformation than AzoAMP-1 at low temperatures. The lack of emission of AzoAMP-2 also indicates that delocalization of the aniline lone pair into the π-system does not contribute to the fluorescence properties as in BDAAB. The composite results confirm the hypothesis that hydrogen bonding in AzoAMP-1 induces a structural rigidity that provides an emissive azobenzene derivative at low temperatures.

Transient Absorption Studies of AzoAMP-1 and AzoAMP-2. The inclusion of electron-donating aniline substituents in AzoAMP-1 and AzoAMP-2 alters the energies of the frontier molecular orbitals involved in isomerization. To confirm that the AzoAMP compound retains excited state photochemistry analogous to that of azobenzene, ultrafast transient absorption spectra of both compounds in the visible spectral region were recorded after laser excitation at 490 nm into their $S_2 \leftarrow S_0$ bands. While the spectral traces for both molecules are weak (Figure 7), the ground state absorption band below ~525 nm clearly bleaches immediately and an $S_n \leftarrow S_1$ feature that maximizes in 600−700 fs appears. This is similar to the transient absorption behavior of azobenzene, which exhibits rapid decay to the S_1 state following $S_2 \leftarrow S_0$ excitation. Like the steady-state $S_2 \leftarrow S_0$ absorption spectrum, the transient absorption spectrum of AzoAMP-1 is sharper and more vibronically resolved than that of AzoAMP-2, which suggests less conformational disorder in both the S_0 and S_1 states for AzoAMP-1 than for AzoAMP-2. The data imply that conformational disorder is induced in the extended π-electron chain by the introduction of the methylamino substituent in AzoAMP-2.

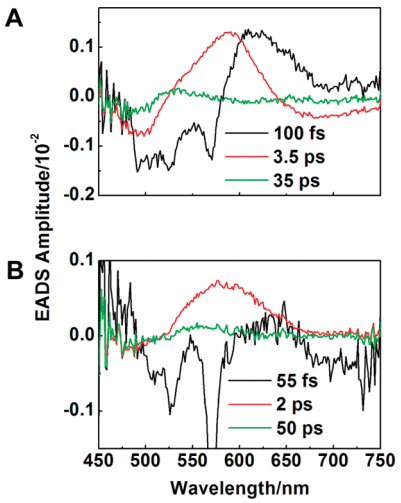

FIGURE 8. Global fitting results (EADS) of transient absorption spectra of AzoAMP-1 (A) and AzoAMP-2 (B).

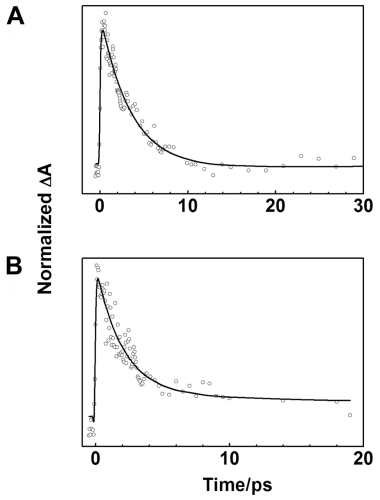

FIGURE 9. Kinetic traces probed at 589 nm for AzoAMP-1 (A) and at 579 nm for AzoAMP-2 (B), with fits obtained from global fitting.

The entire spectral and temporal transient absorption data sets were fit by a global fitting analysis model that assumes a sequential decay of the excited states formed after photoexcitation into S_2 (Figure 8). For both molecules, three evolution associated decay spectra (EADS) kinetic components were needed to fit the data (Figure 9). The first EADS component (black lines in Figure 8) decays in 100 fs for AzoAMP-1 and 55 fs for AzoAMP-2. These lifetimes are shorter than the temporal resolution (~125 fs) of the spectrometer system; nevertheless, the lineshapes in the region below 580 nm display a combination of ground state bleaching and pronounced negative bands associated with Raman scattering from the solvent system. The broad positive band of the first kinetic component sharpens and shifts to shorter wavelength as the line shape evolves into the second EADS component (red lines in Figure 8). This evolution may be attributable to ultrafast vibronic relaxation in the S_1 state. The second EADS profiles are highly characteristic of $S_n \leftarrow S_1$ transient spectral bandshapes of π-electron conjugated molecules and decay in 3.5 ps for AzoAMP-1 and 2 ps for AzoAMP-2. These represent the S_1 lifetimes of the molecules. A third and final EADS component (green lines in Figure 8) is needed for a good fit to the data sets, and these have time constants of 35 and 50 ps for AzoAMP-1 and AzoAMP-2, respectively. These slower components have been assigned by studies on other azobenzenes to vibronic relaxation in the ground state.

AzoAMP-3 and Implications in the Mechanism of Azobenzene Isomerization. While the use of hydrogen bonding alone seems unlikely to provide highly fluorescent azobenzenes at room temperature that compete with the best examples,[35,36] the observations suggest that *ortho*-substituted azobenzene derivatives can be useful probes of the isomerization mechanisms. To further probe for the concerted inversion isomerization mechanism, a monosubsituted version of AzoAMP-1 was prepared.

Reductive amination of 2-pyridinecarboxaldehyde in the presence of 1 equiv of **5** yielded AzoAMP-3 (Scheme 1C). The signal of the single anilino hydrogen atom appears at δ 9.19 ppm in the ^{1}H NMR spectrum, whereas the other two anilino protons appear significantly upfield at δ 5.45 ppm. Isomerization behavior of AzoAMP-3 is very similar to that of AzoAMP-1. Very minimal *trans*→*cis* conversion is observed upon irradiation and thermal *cis*→*trans* isomerization occurs rapidly. This behavior indicates that a hydrogen bonding interaction on one side of the azobenzene is sufficient to prevent isomerization. Both AzoAMP-1 and AzoAMP-3 exhibit some minimal formation of the *cis* isomer upon irradiation, but this may result from direct S_1 excitation, which leads to isomerization via a different mechanism.[48] Since the S_1 and S_2 excitation bands overlap in the AzoAMP compounds and the extinction coefficient for S_1 excitation is very small, it is difficult to probe this process by conventional methods. The emission intensity of AzoAMP-3 (Φ = 0.0008) at 77 K lies between those of AzoAMP-1 and AzoAMP-2.

The composite results from AzoAMP-1, -2, and -3 provide the first systematic demonstration that the concerted inversion provides the best mechanistic explanation for azobenzene isomerization. Like azobenzene, AzoAMP-2 isomerizes because both aryl groups can adopt the collinear arrangement required (Scheme 2). The modest conversion to the *cis* isomer of AzoAMP-2 compared to azobenzene may reflect the steric restrictions of the *ortho* substituents, which might make the collinear C−N=N−C arrangement more difficult to achieve and the *cis* far more sterically congested. In contrast, the hydrogen bonding interactions in AzoAMP-1 and AzoAMP-3 prevent isomerization.

In AzoAMP-1, hydrogen bonding stabilizes both C−N=N bond angles at ~120°, which would not preclude isomerization by rotation after $\pi \rightarrow \pi^*$ (S_2). The time-resolved absorption studies confirm that S_2 excitation is followed by rapid and efficient relaxation to the S_1 state; therefore the lack of isomerization in AzoAMP-1 is most consistent with inhibition of the concerted inversion mechanism. By preventing the aryl groups from adopting the prerequisite collinear arrangement, the hydrogen bonding prevents isomerization. Further evidence for the concerted inversion mechanism can be derived from the photoisomerization experiments with AzoAMP-3. Since 2,2′-diaminoazobenzene isomerizes, weak hydrogen bonding between an azo group and unsubstituted aniline groups does not prevent

SCHEME 2. Concerted Inversion Mechanism in Azobenzene Isomerization

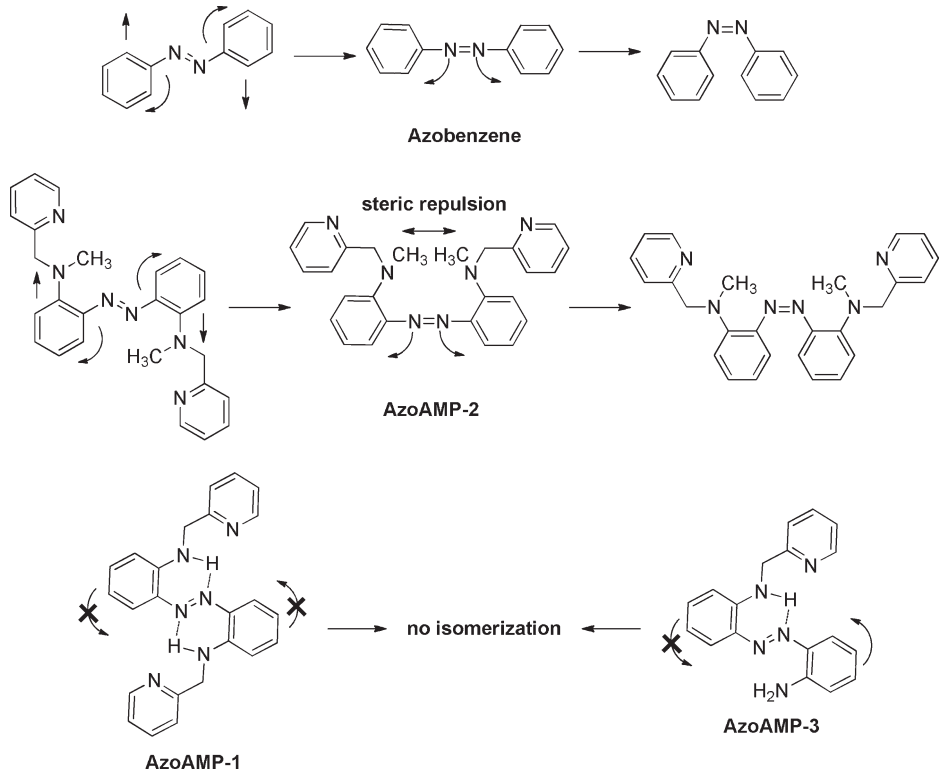

distortions of the C−N=N bond angles. In AzoAMP-3, however, the addition of a single methylpyridine group prevents isomerization. Since only the C−N=N bond adjacent to the AMP group is conformationally restricted, isomerization could occur by inversion of the other aryl group. The lack of isomerization provides experimental confirmation that both aryl groups must move in a concerted process for the inversion to proceed. These systematic steady-state experiments provide strong supporting evidence for the concerted inversion isomerization mechanism, which could only be probed by time-resolved optical spectroscopy and theoretical calculations with unmodified azobenzene.

Conclusions

Incorporation of azobenzene into various biomolecules, polymers, and ligands requires attaching at least one substituent to the phenyl rings. Substitution often changes the electronic properties of the azobenzene and consequently the *trans*→*cis* isomerization behavior. Substituents may also be responsible for higher rates of thermal *cis*→*trans* isomerization, which is undesirable in most applications. Despite numerous attempts, a predictive model that relates the electronic nature, position, and number of substituents on azobenzene with the isomerization has not been completely elucidated. The results described above are the first steps in a more extensive effort to study these structure−photochemistry relationships.

Substitution may also provide interesting photophysical behavior, however. Strong intramolecular hydrogen bonds in AzoAMP-1 and AzoAMP-3 introduce a barrier to photoisomerization. These hydrogen bonds force AzoAMP-1 to adopt a rigid planar structure, which also makes AzoAMP-1 and AzoAMP-3 more emissive than azobenzene at low temperatures. Theoretical calculations demonstrate that these hydrogen bonds prevent isomerization by creating energetic barriers larger than the available kinetic energy upon $S_1 \leftarrow S_2$ conversion. The energy barrier disappears upon elimination of the hydrogen bonds in AzoAMP-2, and the photoisomerization predicted by calculations was confirmed experimentally.

To date, azobenzene derivatives have mostly been exploited for applications that utilize the *trans*→*cis* photoisomerization. With the exception of acting as a fluorescence quencher, fewer applications utilize the other optical properties of azobenzenes. Conjugated polymers containing diphosphene units, the phosphorus analogue of the azo group, have been studied because of their unique spectroscopic properties.[53,54] Using hydrogen bonding to prevent isomerization, new applications of azobenzene derivatives can be explored, such as the development of conjugated polymers with unique properties. Efforts to further delineate the photochemistry of azobenzene derivatives and develop new applications for conformationally restricted azobenzenes are ongoing.

Experimental Section

General Synthetic Procedures. All reagents were purchased from Acros at the highest commercial quality and used without further purification. *N*-Methyl-2-(aminomethyl)pyridine (**7**)[55]

(53) Smith, R. C.; Protasiewicz, J. D. *Eur. J. Inorg. Chem.* **2004**, 998–1006.
(54) Smith, R. C.; Protasiewicz, J. D. *J. Am. Chem. Soc.* **2004**, *126*, 2268–2269.
(55) Seitz, M.; Kaiser, A.; Tereshchenko, A.; Geiger, C.; Uematsu, Y.; Reiser, O. *Tetrahedron* **2006**, *62*, 9973–9980.

and 2,2′-diaminoazobenzene (**5**)[56] were synthesized according to literature procedures. Dichloromethane (CH_2Cl_2) and tetrahydrofuran (THF) were sparged with argon and dried by passage through a Seca solvent purification system. All chromatography and TLC were performed on silica (230−400 mesh) from Silicycle. TLCs were developed with mixtures of EtOAc/MeOH or EtOAc/hexanes and were visualized with 254 and 365 nm light. ^{1}H and ^{13}C NMR spectra were recorded using a 400 MHz NMR instrument, and chemical shifts are reported in ppm on the δ scale relative to tetramethylsilane. IR spectra were recorded on a FT-IR instrument, and the samples were prepared as KBr pellets or thin films on KBr plates. High resolution mass spectra were recorded using a electrospray mass spectrometer operating in positive ion mode.

2,2′-Bis[*N*,*N*′-(2-pyridyl)methyl]diaminoazobenzene (AzoAMP-1, 1). The azobenzene **5** (320 mg, 1.5 mmol) and 2-pyridinecarboxaldehyde (0.29 mL, 3.0 mmol) were combined in CH_2Cl_2 (70 mL), and $NaBH(OAc)_3$ (767 mg, 3.6 mmol) was added. The mixture was stirred at 23 °C for 24 h. Water (40 mL) was added, and the product was extracted into CH_2Cl_2 (3 × 40 mL). The combined organic layers were dried over $MgSO_4$, and the solvent was removed. Flash chromatography on silica (24:1 EtOAc/MeOH) followed by recrystallization (CH_2Cl_2/Et_2O) yielded **1** as red flaky crystals (178 mg, 30.1%). TLC R_f = 0.45 (silica, 49:1 EtOAc:MeOH). Mp = 163−165 °C. ^{1}H NMR (400 MHz, $CDCl_3$) δ 9.03 (s, 2 H), 8.61 (d, J = 4.7 Hz, 2 H), 7.87 (dd, J = 7.8, 1.4 Hz, 2 H), 7.65 (dt, J = 1.6, 7.8 Hz, 2 H), 7.38 (d, J = 7.8 Hz, 2 H), 7.26−7.18 (m, 4H), 6.81 (t, J = 7.2 Hz, 2 H), 6.76 (d, J = 8.2 Hz, 2 H), 4.71 (s, 4 H). ^{13}C NMR (100 MHz, $CDCl_3$) δ 158.3, 149.3, 143.0, 137.3, 137.1, 131.7, 128.0, 122.4, 121.6, 116.6, 112.4, 48.7. IR (neat, cm^{-1}) 3207.9, 3066.7, 3020.8, 2857.9, 2840.7, 1606.5, 1594.5, 1497.6, 1447.7, 1439.2, 1415.9, 1309.9, 1285.9, 1205.4, 1153.2, 1081.1, 1043.9, 993.7, 843.4, 737.5, 671.3. HRMS (+ESI): Calcd for $C_{24}H_{22}N_6H^+$, 395.1984; Found, 395.1968.

Methyl-(2-nitro-phenyl)-pyridin-2-ylmethyl-amine (8). The amine **7** (2.00 g, 16.4 mmol) and 2-bromonitrobenzene (3.30 g, 18.0 mmol, **6**) were combined in dry 1,4-dioxane (80 mL) and K_2CO_3 (8.48 g, 53.3 mmol) was added. The mixture was refluxed at 100 °C for 72 h. Water (20 mL) was added and the product was extracted into CH_2Cl_2 (3 × 40 mL). The combined organic layers were dried over $MgSO_4$ and the solvent was removed. Flash chromatography on silica (EtOAc) yielded **7** as a yellow-orange oil (721 mg, 18.0%). TLC R_f = 0.51 (silica, EtOAc). ^{1}H NMR (400 MHz, $CDCl_3$) δ 8.57 (d, J = 4.8 Hz, 1 H), 7.77 (dd, J = 8.1, 1.0 Hz, 1 H), 7.71 (dt, J = 7.7, 1.3 Hz, 1 H), 7.44 (dd, J = 7.9, 0.6 Hz, 1 H), 7.39 (t, J = 7.3 Hz, 1 H), 7.22 (dd, J = 7.0, 5.1 Hz, 1 H), 7.14 (d, J = 8.4 Hz, 1 H), 6.93 (t, J = 7.4 Hz, 1 H), 4.56 (s, 2 H), 2.88 (s, 3 H). ^{13}C NMR (100 MHz, $CDCl_3$) δ 157.7, 149.2, 145.8, 141.3, 137.4, 133.4, 126.5, 122.6, 122.2, 120.4, 119.9, 60.6, 41.5. IR (neat, cm^{-1}) 3065.1, 3008.2, 2926.1, 1604.2, 1589.7, 1566.8, 1433.0, 1342.1, 1290.1, 1231.9, 1214.8, 1193.1, 1114.1, 992.7, 939.1, 852.4, 741.6, 708.3. HRMS (+ESI): calcd for $C_{13}H_{13}N_3O_2H^+$, 244.1086; found, 244.1119.

2,2′-Bis[*N*,*N*′-methyl-*N*,*N*′-(2-pyridyl)methyl]aminoazobenzene (AzoAMP-2, 2). The amine **7** (400 mg, 1.64 mmol) was dissolved in THF (80 mL) and treated with $LiAlH_4$ (125 mg, 3.28 mmol). The mixture was stirred at 23 °C for 2 h. Water (20 mL) was added, and the product was extracted into CH_2Cl_2 (3 × 40 mL). The combined organic layers were dried over $MgSO_4$, and the solvent was removed. Flash chromatography on silica (48:2 EtOAc/MeOH) yielded **2** as a red oil (43.4 mg, 12.5%). TLC R_f = 0.44 (silica, 48:2 EtOAc/MeOH). ^{1}H NMR (400 MHz, $CDCl_3$) δ 8.56 (d, J = 4.4 Hz, 2 H), 7.62 (dt, J = 7.8, 1.6 Hz, 2 H), 7.53 (d, J = 7.7 Hz, 2 H), 7.24−7.15 (m, 4 H), 7.06−7.01 (m, 4 H), 6.59 (dt, J = 7.7, 1.0 Hz, 2 H), 4.76 (s, 4H), 3.06 (s, 6H). ^{13}C NMR (100 MHz, $CDCl_3$) δ 160.1, 150.1, 149.3, 143.7, 136.7, 131.2, 122.0, 121.9, 119.8, 118.1, 117.7, 64.3, 40.9. IR (neat, cm^{-1}) 3058.9, 2946.4, 2869.9, 2802.9, 1588.7, 1568.1, 1484.5, 1431.4, 1358.0, 1304.0, 1184.3, 1159.8, 1100.5, 1046.2, 991.8, 936.6, 747.3. HRMS (+ESI): calcd for $C_{26}H_{26}N_6Na^+$, 445.2117; found, 445.2103.

2-Amino-2′-[*N*-(2-pyridyl)methylamino]azobenzene (AzoAMP-3, 3). The diamine **5** (180 mg, 0.85 mmol), 2-pyridinecarboxaldehyde (81 μL, 0.85 mmol), and $NaBH(OAc)_3$ (360 mg, 1.7 mmol) were combined in CH_2Cl_2 (20 mL). The reaction mixture was stirred at 23 °C for 18 h. Water (20 mL) was added, and the product was extracted into CH_2Cl_2 (3 × 40 mL). The combined organic layers were dried over $MgSO_4$, and the solvent was removed. TLC showed a mixture of 2,2′-diaminoazobenzene, AzoAMP-1, and AzoAMP-3. Addition of 6:4 EtOAc/hexanes caused AzoAMP-1 to precipitate. Flash chromatography on silica (6:4 EtOAc/hexanes) yielded AzoAMP-3 as a viscous red oil (11 mg, 4.0%). TLC R_f = 0.62 (silica, 19:1 EtOAc/MeOH). ^{1}H NMR (400 MHz, $CDCl_3$) δ 9.19 (s, 1 H), 8.64 (d, J = 4.3 Hz, 1 H), 7.82 (dt, J = 1.5, 8.2 Hz, 2 H), 7.68 (dt, J = 1.7, 7.7 Hz, 1 H), 7.36 (d, J = 7.7 Hz, 1 H), 7.29−7.17 (m, 3 H), 6.86−6.79 (m, 4 H), 5.45 (s, 2 H), 4.69 (s, 2 H). ^{13}C NMR (100 MHz, $CDCl_3$) δ 157.7, 149.2, 143.6, 142.7, 138.2, 137.2, 137.0, 131.9, 131.2, 129.6, 123.4, 122.5, 121.8, 117.8, 117.2, 116.4, 112.3, 48.5. IR (neat, cm^{-1}) 3456.4, 3342.9, 3064.5, 2921.8, 2849.4, 1607.1, 1561.2, 1507.7, 1483.7, 1448.6, 1423.5, 1387.5, 1330.8, 1260.6, 1234.4, 1211.4, 1153.6, 1082.2, 1048.6, 908.2, 798.5, 758.2, 735.8, 579.4. HRMS (+ESI): calcd for $C_{18}H_{17}N_5Na^+$, 326.1382; found, 326.1354.

Crystals of AzoAMP-1. A 15 mg of sample of AzoAMP-1 was dissolved in the minimum amount of boiling acetonitrile. The resulting solution was allowed to stand at 23 °C for 30 min and placed in an Et_2O diffusion chamber where single crystals gradually formed from solution.

Collection and Reduction of X-ray Data. Structural analysis was carried out in the X-ray Crystallographic Facility at Yale University. Crystals were covered with oil and an orange rod crystal of $N_6C_{24}H_{22}$ with approximate dimensions of 0.50 mm × 0.25 mm × 0.20 mm was mounted on a glass fiber at room temperature and transferred to a Rigaku RAXIS RAPID imaging plate area detector with graphite monochromated Cu Kα radiation (λ = 1.54187 Å) controlled by a PC running the Rigaku CrystalClear software package.[57] The data were collected at a temperature of −50 ± 1 °C to a maximum 2θ value of 55°. The data were corrected for Lorentz and polarization effects. The structure was solved by direct methods[58] and expanded using Fourier techniques.[59] The space group was determined by examining systematic absences and confirmed by the successful solution and refinement of the structure. The non-hydrogen atoms were refined anisotropically. Hydrogen atoms were refined using the riding model. All calculations were performed using the CrystalStructure[60] crystallographic software package except for refinement, which was performed using SHELXL-97.[58] Relevant crystallographic information is summarized in Tables 1 and 2, and the 50% thermal ellipsoid plot is shown in Figure 3A.

General Spectroscopic Methods. All solutions were prepared with spectrophotometric grade solvents. Graphs were manipulated and equations calculated by using Kaleidagraph 4.0.

(56) Crank, G.; Makin, M. I. H. *Aust. J. Chem.* **1984**, *37*, 845–55.

(57) *CrystalClear and CrystalStructure*; Rigaku/MSC: The Woodlands, TX, 2005.

(58) Sheldrick, G. M. *SHELX97, Programs for Crystal Structure Analysis*; Universität Göttingen, Göttingen, Germany, 1997.

(59) Beurskens, P. T.; Admiraal, G.; Beurskens, G.; Bosman, W. P.; de Gelder, R.; Israel, R.; Smits, J. M. M. *DIRDIF99*; University of Nijmegen: The Netherlands, 1999.

(60) *CrystalStructure 3.8: Crystal Structure Analysis Package*; Rigaku and Rigaku Americas: The Woodlands, TX, 2007.

TABLE 1. Crystallographic Parameters for AzoAMP-1 (1)

formula	$N_6C_{24}H_{22}$
formula wt.	394.48
space group	$P2_{1/c}$
a, Å	10.1401(11)
b, Å	13.6843(15)
c, Å	7.3008(8)
β, deg	95.328(2)
V, Å^3	1008.68(19)
Z	2
ρ_{calcd} (g cm^{-3})	1.299
absorp coeff (cm^{-1})	0.808
temp, K	223
total no. data	10199
no. unique data	2301
obs. data[a]	2301
no. parameters	141
R, %[b]	0.0490
wR2, %[c]	0.1294
max/min peaks, e/Å	0.20, −0.17

[a]Observation criterion: $I > 2\sigma(I)$. [b]$R = \Sigma||F_o| - |F_c||/\Sigma|Fo|$. [c]wR2 = $[\Sigma(w(F_o^2 - F_c^2)^2)/\Sigma w(F_o^2)^2]^{1/2}$

TABLE 2. Selected Interatomic Distances (Å) and Angles (deg)[a]

bond lengths		bond angles	
N(3)−N(3)	1.2793(15)	N(3)−N(3)−C(12)	116.87(10)
N(3)−C(12)	1.4127(16)	N(3)−C(12)−C(7)	126.89(11)
N(2)−C(7)	1.3573(18)	C(12)−C(7)−N(2)	121.64(11)
N(2)−C(6)	1.4434(18)	C(7)−N(2)−H(2A)	120.1(11)
N(2)−H(2A)	0.865(15)	H(2A)−N(2)−C(6)	115.3(11)
N(1)−H(2A)	2.219	N(2)−C(6)−C(5)	110.70(10)
N(3)−H(2A)	2.046	C(6)−C(5)−N(1)	118.15(12)

[a]Number in parentheses are estimated standard deviations in the last digit(s). Atom labels are provided in Figure 3A.

Absorption spectra were recorded on a UV−vis spectrophotometer under the control of a PC running the manufacturer supplied software package. Spectra were routinely acquired at 25 °C, in 1-cm path length quartz cuvettes with a total volume of 3.0 mL. Fluorescence spectra were recorded on a spectrophotometer under the control of a PC running the manufacturer supplied software package. Excitation was provided by a 150 W Xe lamp operating at a current of 5 A. Spectra were routinely acquired at 25 °C, in 1 cm quartz cuvette with a total volume of 3.0 mL using, unless otherwise stated, 10 nm slit widths, and a photomultiplier tube power of 700 V. Photoisomerization experiments were performed at 25 °C, in 1-cm path length quartz cuvettes illuminated by a 150 W Xe lamp of a spectrophotometer with emission wavelength set to λ_{max} of the AzoAMP species.

Irradiation of AzoAMP-1 and AzoAMP-3. Solutions of AzoAMP (10 and 25 μM) were irradiated at λ_{max} in hexanes, benzene, Et_2O, THF, EtOAc, DMF, DMSO, MeOH, and Et_2O/EtOH (1:1). Aqueous solutions of AzoAMP-1 (pH 1, 4, 7, 10, and 14 and in concentrated HCl) were also irradiated. In DMF the excitation wavelength was varied between 250 and 600 nm (10 nm intervals between 450 and 550 nm, 20 nm intervals outside this range). Several different excitation wavelengths were tried in water, MeOH, and DMSO. No significant isomerization was observed under any of these conditions.

Isomerization of AzoAMP-2. A 1.0-mL aliquot of EtOH and a 1.0-mL aliquot of Et_2O were placed in a cuvette and the background UV−vis spectrum was recorded. A 4-μL aliquot of an AzoAMP-2 solution (5.00 mM) was added to achieve a final concentration of 10 μM, and the absorption spectrum was recorded. The cuvette was irradiated at 451 nm, and spectra were recorded at 1 min intervals. No additional changes in absorbance were observed after 15 min. The solution was kept in the dark, and absorbance was recorded at 1 min intervals to monitor the *cis* to *trans* thermal isomerization.

Quantum Yield of Photoisomerization of AzoAMP-2. Intensity of Source. To determine the intensity of the radiation source, a 1.0-mL aliquot of a 10 mM potassium ferrioxalate solution was placed in an NMR tube and irradiated with 460 nm wavelength radiation for 5 min. This results in the reduction of Fe(III) oxalate to Fe(II) oxalate. The irradiated solution was combined with 15 mg of ferrozine (3 equiv), resulting in the formation of a reddish-purple solution containing $[Fe(ferrozine)_3]^{2+}$, which has a molar absorption coefficient of 27,900 cm^{-1} M^{-1} at 563 nm. A 100-μL aliquot of the resulting solution was diluted by a factor of 30, and its absorbance was measured at 563 nm. The concentration of Fe(II) produced by the reduction of Fe(III) oxalate is given by eq 1 where ε_{563} = 27,900 cm^{-1} M^{-1}.

$$[\text{Fe(II)}] = \frac{A_{563} \times 30}{\varepsilon_{563}} \quad (1)$$

The intensity of the radiation source at 460 nm is given by eq 2 where Φ = 1.25.

$$\text{intensity (quanta s}^{-1}\text{L}^{-1}) = \frac{[\text{Fe(II)}]/\text{irradiation time}}{\Phi_{460}} N_A \quad (2)$$

Quantum Yield of Photoisomerization. A 1.3-mg sample of AzoAMP-2 was dissolved in 1.0 mL of $CDCl_3$ to achieve a final concentration of 3.1 mM. The solution was transferred into an NMR tube, and the ^{1}H NMR spectrum of the solution was recorded. The NMR tube was irradiated at 460 nm for 30 min, and the ^{1}H NMR spectrum of the solution was recorded. Growth of new peaks was observed near NCH_3 resonance and NCH_2Py resonance of the ^{1}H NMR spectrum. The [*cis*]:[*trans*] isomer ratio was calculated using integrated peak areas of the NCH_3 resonance.

The quantum yield of photoisomerization (Φ) of AzoAMP-2 is obtained by solving eq 3:

$$\Phi = \frac{\text{Change in [AzoMAP-2]/irradiation time}}{\text{intensity of source}} N_A \quad (3)$$

Low-Temperature Absorption Spectroscopy. A 1.5-mL aliquot of EtOH and a 1.5-mL aliquot of Et_2O were placed in a cuvette, and the background UV−vis spectrum was recorded. A 20-μL aliquot of an AzoAMP solution (5.00 mM) was added to achieve a final concentration of 50 μM, and the spectrum was recorded. The cuvette containing the AzoAMP solution was immersed in liquid N_2 to obtain a transparent glass and its absorption spectrum was recorded.

Low-Temperature Fluorescence Spectroscopy. A 1.0-mL aliquot of EtOH and a 1.0-mL aliquot of Et_2O were placed in a quartz cuvette. A 40-μL aliquot of an AzoAMP solution (5.00 mM) was added to achieve a final concentration of 100 μM, and the fluorescence spectrum was recorded. The cuvette containing the AzoAMP solution was immersed in liquid N_2 to obtain a transparent glass, and its fluorescence spectrum was recorded.

Quantum Yield of Fluorescence. Quantum yields were calculated by measuring the integrated emission area of the corrected spectra and comparing that value to the area measured for fluorescein in 0.1 N NaOH when excited at 490 nm (Φ_{fl} = 0.85). The quantum yield of AzoAMP-1 (100 μM solution in 1:1 EtOH/Et_2O frozen in liquid N_2) was then calculated using eq 1, where F represents the area under the emission spectra for the standard and sample, η is the refractive index of the solvent, and A is the absorbance at the excitation wavelength selected for

the standard and sample. Emission was integrated between 502 and 700 nm.

$$\Phi_{fl}^{sample} = \Phi_{fl}^{standard}\left(\frac{F^{sample}}{F^{standard}}\right)\left(\frac{\eta^{sample}}{\eta^{standard}}\right)\left(\frac{A^{standard}}{A^{sample}}\right) \quad (4)$$

Computational Methods. Ground and excited states were obtained using density functional theory (DFT) and time-dependent DFT with the hybrid functional B3LYP and the split-valence double-ζ basis set 6-31g**. The quantum chemistry package Jaguar was used for all calculations.[61]

Ultrafast Time-Resolved Spectroscopic Methods. Transient absorption spectra were recorded using a femtosecond laser spectrometer system previously described.[62] The transient experiments were done at room temperature on AzoAMP-1 and AzoAMP-2 ethanol/ether (1:1, v/v) and adjusted to an optical density of ∼1.0 in a 2 mm path length quartz cuvette at the excitation wavelength of 490 nm. The pump laser beam had an energy of 1 μJ/pulse and a spot diameter of 1 mm corresponding to an intensity of $\sim 3.2 \times 10^{14}$ photons/pulse/cm^2. Steady-state absorption spectra were recorded after each experiment to check the integrity of the samples. Surface Xplorer Pro (v.1.1.0.17) software was used for chirp correction of the spectral data sets and for the determination of the number of principal components via single value decomposition (SVD). ASUfit version 3.0 software was used for global fitting analysis. The goodness of fit was checked from the values of the residuals matrix and chi square (χ^2).

(61) *Jaguar 7.5*; Schrodinger, LLC: New York, NY, 2008.

(62) Ilagan, R. P.; Christensen, R. L.; Chapp, T. W.; Gibson, G. N.; Pascher, T.; Polivka, T.; Frank, H. A. *J. Phys. Chem. A* **2005**, *109*, 3120–3127.

Note Added after ASAP Publication. This paper was published on June 14, 2010, with several typographic errors in the Introduction and Results sections. The corrected version was reposted on June 16, 2010.

Acknowledgment. We thank Professor Challa Vijaya Kumar for insightful discussions. Work in the laboratories of S.C.B. and J.G. was supported by the University of Connecticut. Work in the laboratory of H.A.F. is supported by a grant from the National Science Foundation (MCB-0913022) and by the University of Connecticut Research Foundation. W.I. was supported by the University of Connecticut Department of Chemistry NSF-REU program (CHE-0754580).

Supporting Information Available: ^{1}H and ^{13}C NMR spectra for all new compounds synthesized; absorption of AzoAMP-1 and AzoAMP-2 at room temperature and 77 K; changes in the absorption spectrum of AzoAMP-1 upon irradiation; changes in the absorption spectrum of AzoAMP-2 upon irradiation; thermal recovery of *trans*-AzoAMP-2 after removal from light source; titration of AzoAMP-2 with Zn^{2+}; ^{1}H NMR of AzoAMP-2 before and after irradiation; changes in the absorption spectrum of AzoAMP-3 upon irradiation; additional calculated energy surfaces for inversion, rotation, and concerted inversion pathways for azobenzene, AzoAMP-1, and AzoAMP-2; changes in the absorption spectrum of 2,2′-diaminoazobenzene upon irradiation; complete tables of X-ray data and fully labeled ORTEP diagram; transient spectrum of ethanol/ether (1:1, v/v) recorded at a delay time of 100 fs after laser excitation. This material is available free of charge via the Internet at http://pubs.acs.org.